RSC Advances

PAPER

View Article Online
View Journal | View Issue

Cite this: *RSC Adv.*, 2022, **12**, 21875

Colorimetric sensing of glucose and GSH using core–shell Cu/Au nanoparticles with peroxidase mimicking activity

Ruimeng Sun, Ruijuan Lv, Yang Zhang, Ting Du, Yuhan Li, Lixia Chen and Yanfei Qi *

Received 13th April 2022
Accepted 6th July 2022

DOI: 10.1039/d2ra02375j

rsc.li/rsc-advances

The catalytic properties of bimetallic nanoparticles have been widely studied by researchers in many fields. In this paper, core–shell Cu/Au nanoparticles (Cu/Au NPs) were synthesized by a simple and mild one-pot method, and their peroxidase activity was proved by catalyzing the oxidation of 3,3′,5,5′-tetramethylbenzidine (TMB) with color change to blue. The change of solution color and absorbance strongly depends on the concentration of H_2O_2, so it can be used for direct detection of H_2O_2 and indirect detection of glucose. What's more, GSH can efficiently react with the hydroxyl radicals from H_2O_2 catalyzed by core–shell Cu/Au NPs to inhibit the production of ox-TMB. Thus, the concentration of GSH can be determined by the decrease in the absorbance of the solution at 652 nm. The results showed that our proposed strategy had good detection range and detection limit for the detection of glucose and GSH. This method has been used in the detection of practical samples and has great application potential in environmental monitoring and clinical diagnosis.

Introduction

In the past decades, the synthesis and application of single metal nanoparticles (NPs) have attracted extensive attention in the fields of analytical medicine, catalysis, chemistry and so on.[1–4] In contrast, bimetallic nanoparticles composed of two different metal elements have significantly improved physical and chemical properties (such as unique optical, electronic and catalytic properties), which made researchers gradually focus on bimetallic nanomaterials for the detection of various substances.[5–7] Among the reported nanoparticles, gold-based nanoparticles have become one of the most attractive materials because of their intrinsic enzyme activity, such as peroxidase activity based on chitosan-AuNPs for the detection of glucose in serum,[8] labeling-free sulfate colorimetric sensing based on inhibition of peroxidase like activity of cysteamine-AuNPs,[9] peroxidase mimics based on BSA-AuNCs for colorimetric detection of Ag^+,[10] nano-enzyme activity of histidine-Au nanoclusters for the detection of Cu^{2+} and histidine,[11] gold core/ceria shell based nano-enzyme activity for glucose detection[12] and a nanoceria PTA*-AuNP composite[13] and 11-MUA coated gold-core CeO_2-shell NP-based nanozyme[14] with high peroxidase activity. In order to further improve the catalytic properties and applications of gold-based nanomaterials, their composites have been widely studied, such as Au@TiO_2 yolk–shell structure,[15] $ZnFe_2O_4$@Au,[16] Cu@Au NPs[5,6] and Au@Ag.[17] Besides, as a cheap alternative to precious metals, copper-based semiconductor nanomaterials have been widely studied because of their well-defined shape characteristics[18] and peroxidase activity, such as Cu NCs[19] and CuS NCs.[20] Therefore, the excellent properties of gold and copper were combined for the construction of sensors to be widely studied, such as the detection of chromium (III) based on Cu/Au NCs,[21] the detection of lysozyme[6] and cancer cells[7] based on the special reaction of Cu/Au NPs to iodine and the electrochemical detection of *Escherichia coli* based on Cu/Au NPs.[5] Inspired by these previous works, we prepared core–shell Cu/Au NPs and investigated their peroxidase activities.

Hydrogen peroxide (H_2O_2), as an important oxidant, is not only proved to be a by-product of metabolic oxidation process, but also plays a significant role in food production, biomedicine, pharmacy, industry and environment. It is harmful to organisms when the concentration reaches 0.5 mmol L^{-1}.[22–24] Thus, the high sensitivity detection of H_2O_2 is significant in many fields.[25] In addition, as the main energy of human body, glucose is of great significance in physiological process and is also widely used in food and pharmaceutical industry.[23,26] However, the disorder of glucose levels in the blood can lead to diabetes.[27] Thus, the development of sensitive and selective glucose detection methods plays an important role in monitoring diseases and preventing complications, such as kidney failure, hypertension, stroke, heart disease and blindness and so on.[28] In recent years, different glucose detection methods have been reported, such as colorimetry,[29] fluorescence,[30,31] surface enhanced Raman spectroscopy (SERS)[32] and electrochemical methods.[33] Most glucose detection methods are based on the oxidation or reduction of H_2O_2 produced by enzymatic

School of Public Health, Jilin University, Changchun 130021, Jilin, P. R. China. E-mail: qiyanfei@jlu.edu.cn

method.[34–36] Compared with natural enzymes, nano-enzymes have the advantages of high denaturation resistance, high stability, low cost and easy storage. They are attractive and promising candidate enzymes in the field of chemical sensing.[37] It has been widely reported to develop colorimetric methods for the detection of hydrogen peroxide by using the peroxidase like activity of nano-materials.[23,29,38] Cu/Au NPs were composed of two metal atoms with different properties, which have special sensing ability. Consequently, Cu/Au NPs with peroxidase activity were used for the sensitive detection of hydrogen peroxide and glucose.

Glutathione is a tripeptide containing γ-amide bond (γ-) and sulfhydryl (-SH), composed of glutamate, cysteine and glycine, and exist in almost every cell of the body.[39] Glutathione can be divided into reduced L-glutathione (GSH) and oxidized L-glutathione (GSSG), and help maintain normal immune system function, and has antioxidant effect, integration and detoxification effect.[39–41] More importantly, GSH can protect the normal oxygen transport function of hemoglobin by reducing methemoglobin to hemoglobin and combining with oxidant to generate GSSG and water.[42–44] Besides, GSH can eliminate redundant free radicals (ROS) in human body, remove toxic substances in human body, and even regulate gene expression.[45,46] The level of GSH is closely related to a variety of clinical diseases, such as aging, cancer, AIDS, diabetes, liver injury, cardiovascular disease and Alzheimer's disease.[47,48] Hence, it is extremely important to develop a simple and fast GSH detection method.

In this paper, we established a simple colorimetric assay for the detection of H_2O_2, glucose and GSH based on the peroxidase-like activity of core–shell Cu/Au NPs (Scheme 1). In this assay, the effects of pH, temperature and reaction time have been investigated. Under the optimal reaction conditions, the resulting biosensor exhibited good responses to H_2O_2, glucose and GSH. In addition, it displayed excellent anti-interference ability and fast response in the actual sample.

Materials and methods

Chemicals and materials

All the chemicals used were of analytical grade without further purification. $CuSO_4 \cdot 5H_2O$ were purchased from Tianjin Guangfu Fine Chemical Research Institute (Tianjin, China). Hydrogen tetrachloroaurate (III) trihydrate ($HAuCl_4 \cdot 3H_2O$) was provided by Alfa Aesar (Shanghai, China). Sodium borohydride ($NaBH_4$) and α-Lactose monohydrate were obtained from Guoyao Chemical Research Institute (Shanghai, China). 3,3′,5,5′-Tetramethylbenzidine (TMB) was purchased from Tokyo Chemical Industry Co. Ltd (Tokyo, Japan). Glucose oxidase (GOx) was obtained from Aladdin Reagent Co. Ltd (Shanghai, China). L-glutathione was provided by J&K Scientific Ltd (Beijing, China). Sodium acetate trihydrate ($CH_3COONa \cdot 3H_2O$, NaAc), Acetic acid (CH_3COOH, HAc), sodium citrate, KI, glucose and hydrogen peroxide (H_2O_2, 30%) were purchased from Beijing Chemical Works (Beijing, China). L-arginine (L-Arg), L-alanine (L-Ala), L-Lysine (L-Lys), D-alanine (D-Ala), L-valine (L-Val) and L-aspartic acid (L-Asp) were purchased from Shanghai HuiShi Biological Technology Co. Ltd (Shanghai, China). The water used in the experiments was purified. The resistivity (ρ) of water was 18 MΩ cm.

Apparatus and characterization

The morphologies of the samples were observed using TEM (JEM-1011, Japan) with a working voltage at 100 kV. Particles' size (nm) and surface charge (ζ-potential, mV) were characterized using Zetasizer (Nano-ZS90) dynamic light scattering detector (Malvern Instruments Ltd, Worcestershire, UK). The UV/vis spectra were recorded in the range of 400 nm–800 nm on a TU 1810 UV-vis spectrophotometer (Beijing Persee General Instrument Co. Ltd, Beijing, China) or Microplate reader (Bio-Tek, Winooski, Vermont, USA). 1 cm path length quartz cuvette or 96-well microplates were used in the experiment. The pH

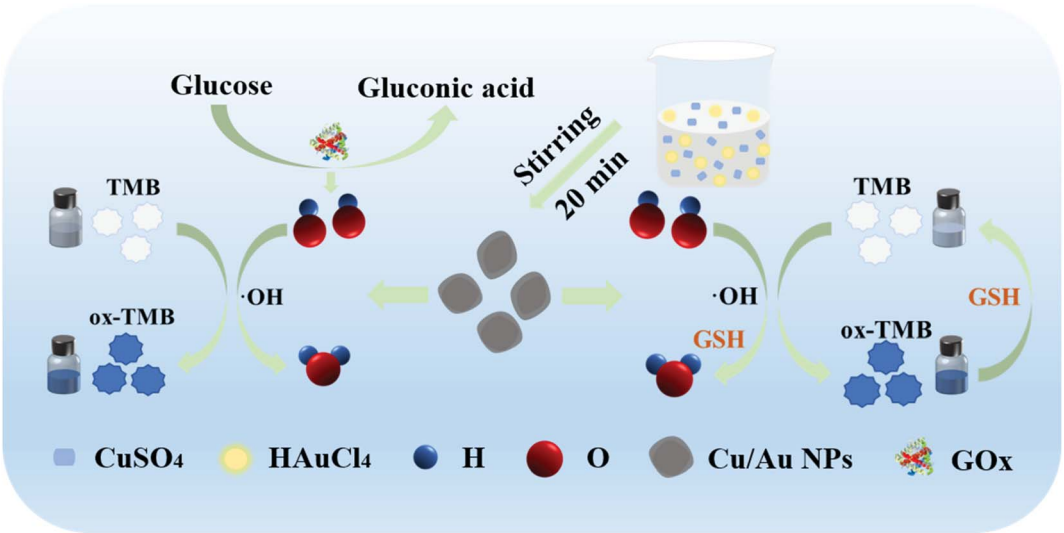

Scheme 1 Illustration of the preparation process for core–shell Cu/Au NPs and sensing assay H_2O_2, glucose and GSH.

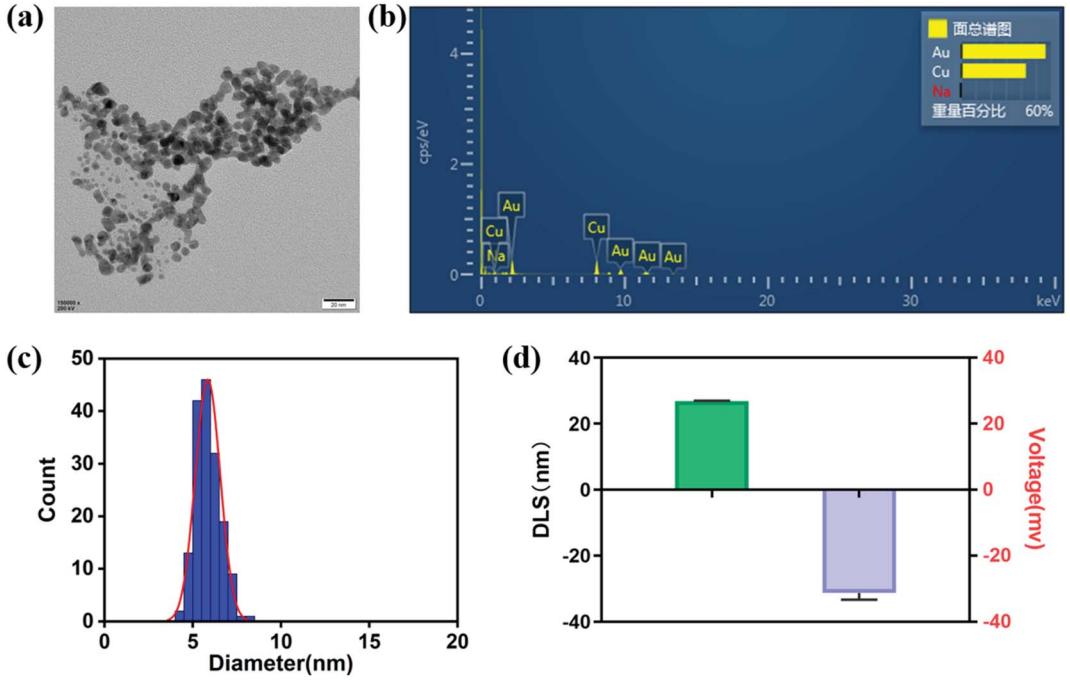

Fig. 1 (a) TEM, (b) EDS, (c) particle size distribution, (d) size and ζ-potential of core–shell Cu/Au NPs. Error bars represent the standard deviation of three repeated measurements.

measurements were performed by a PHS-25 pH meter (Shanghai INESA Scientific Instrument Co. Ltd, Shanghai, China).

Synthesis of core–shell Cu/Au NPs

We synthesized core–shell Cu/Au NPs according to the methods reported in the literature.[49] Briefly, a beaker containing 20 mL of water was added with 50 μL of $CuSO_4 \cdot 5H_2O$ (0.1 M) and 50 μL of sodium citrate (0.1 M) at room temperature. Subsequently, 1 mL of freshly prepared $NaBH_4$ (3.8 mg in 4 mL of H_2O) was quickly injected into the stirring system in ambient condition. After 15 min, $HAuCl_4$ solution (50 μL, 0.1 M) was added to the rapid stirring system and maintained 20 min. The obtained core–shell Cu/Au NPs solution was stored at 4 °C for 24 h before its further application.

Characterization of iodide-responsive core–shell Cu/Au NPs

Different concentrations of KI were mixed with 270 μL of core–shell Cu/Au NPs, the mixed solution was allowed to react for 25 min at room temperature. Subsequently, the spectra were obtained using Microplate reader (BioTek, Winooski, Vermont, USA).

Peroxidase-mimicking catalytic activity

By measuring the formation of ox-TMB at 652 nm by UV/vis spectroscopy, the peroxidase-like catalysis of core–shell Cu/Au

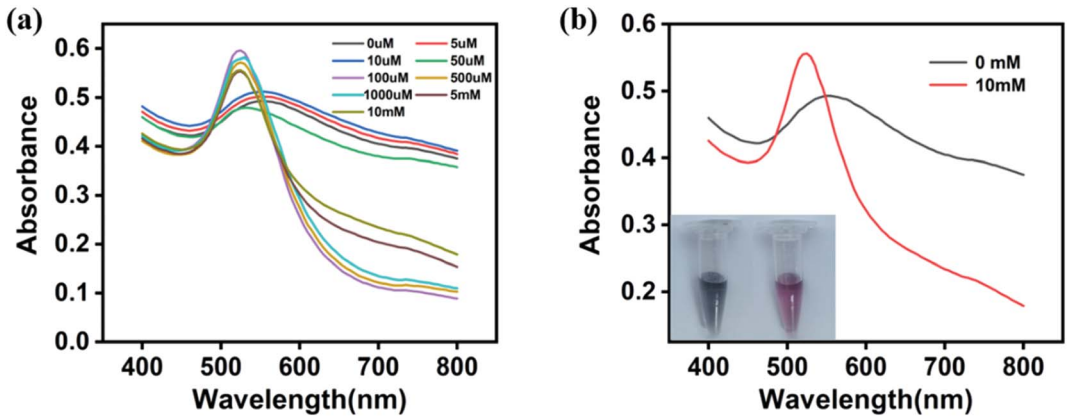

Fig. 2 (a) UV-vis absorption spectra of the solution in presence of iodide with different concentrations (0–10 mM); (b) photos and UV-vis absorption spectra of the solution containing 0/10 mM iodide, respectively (Inset: Color changes of core–shell Cu/Au NPs with 0 mM and 10 mM KI).

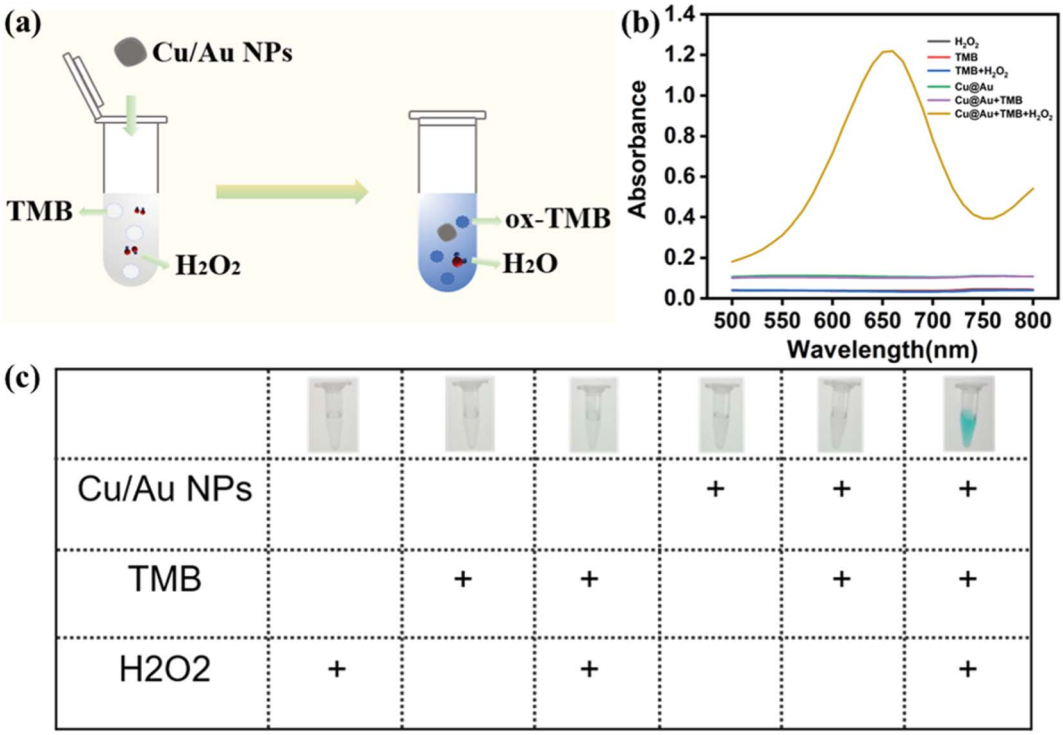

Fig. 3 (a) Schematic of the enzyme-like performance of core–shell Cu/Au NPs. (b) UV-vis absorbance spectrum of the core–shell Cu/Au NPs, TMB and H_2O_2 reaction solutions and controls. (c) Visual photographs of varied control systems.

NPs was studied by spectrophotometry. In details, 40 μL 65 μg mL^{-1} core–shell Cu/Au NPs and 96 μL 1.5 mM TMB were first added to 152 μL HAc-NaAc buffer (pH 5) and followed to be mixed thoroughly with 12 μL H_2O_2.

Steady-state kinetic assay

The steady-state kinetics of Cu/Au NPs were carried out using 100 μL 65 μg mL^{-1} Cu/Au NPs at the optimal condition by varying the concentration of H_2O_2 (0–20 mM) or TMB (0–6.4 mM) one at a time. The absorbance values were measured at 652 nm by using a multi-well plate reader (BioTek, Winooski, Vermont, USA).

According to the Michaelis–Menten equation, $V_0 = V_{max}[S]/(Km+[S])$, the kinetic parameters of catalytic activity were estimated by the initial rate method, where V_0, V_{max} and $[S]$ represent the initial rate, maximum reaction rate and substrate concentration of the reaction, respectively. V_{max} and K_m are also calculated from the Lineweaver–Burk double-reciprocal plot. By the Beer–Lambert law ($A = \varepsilon bc$), the absorbance signal was converted into concentration, where ε = 39 000 M^{-1} cm^{-1} at 652 nm for the oxidized TMB.[27]

Optimization of reaction conditions

To obtain the best detection performance, the pH (from 3 to 8) and temperature (from 25–75 °C) of the reaction system were

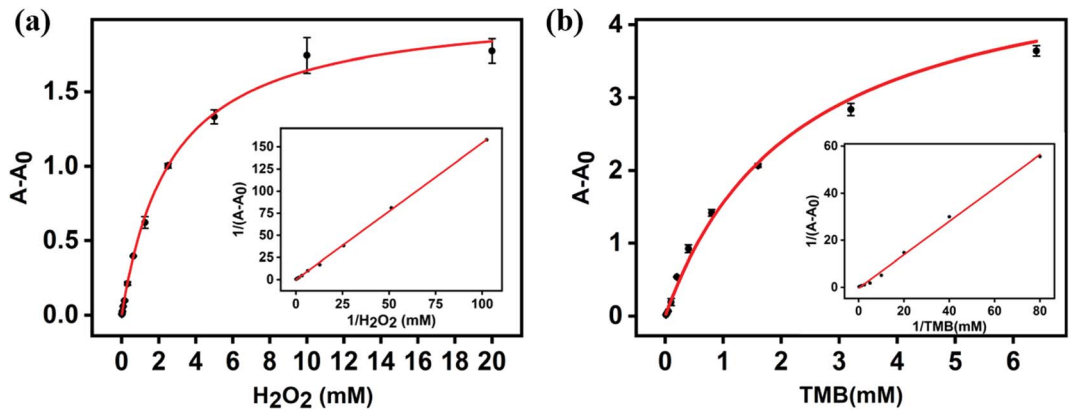

Fig. 4 (a, b) Steady-state kinetic assays of core–shell Cu/Au NPs. Insets are the Lineweaver–Burk plots of the double reciprocal of the Michaelis–Menten equations.

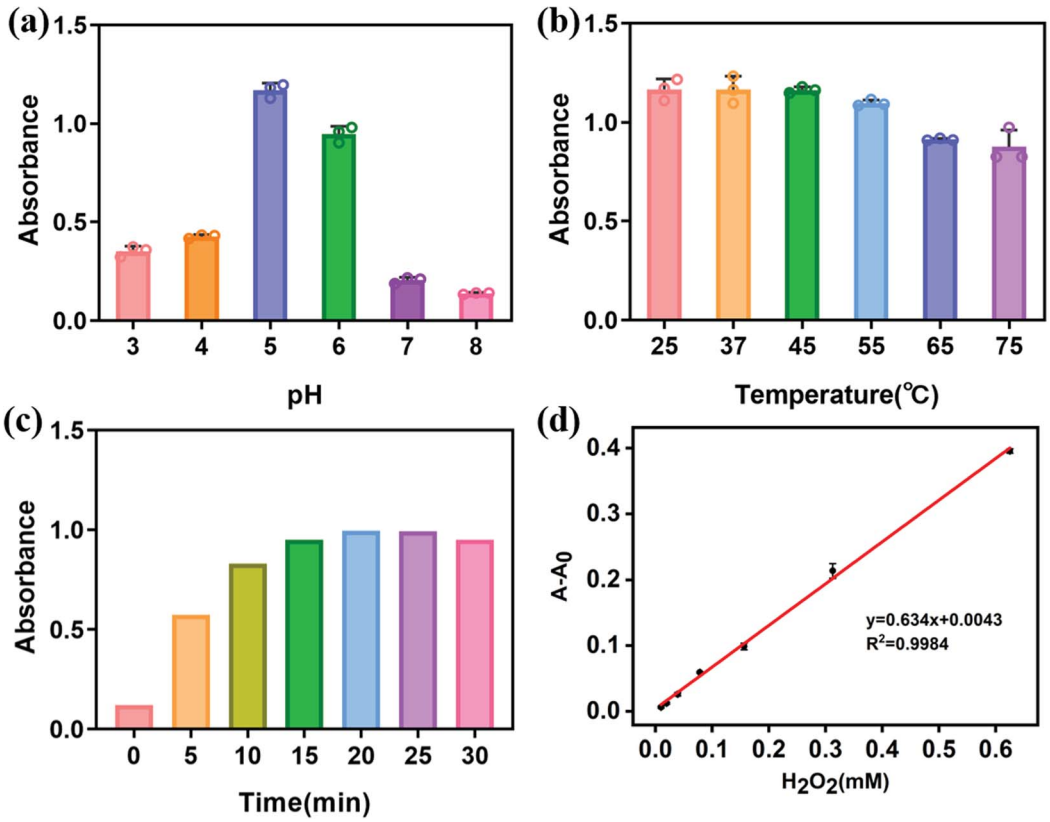

Fig. 5 Optimization of variable experimental factors of colorimetric detection; (a) pH; (b) reaction temperature; (c) reaction time; (d) the linear range of H_2O_2 colorimetric detection. Error bars represent the standard deviation of three repeated measurements.

Table 1 Comparison of different colorimetric systems for the detection of H_2O_2 and glucose

Nanozymes	Linear range	Limit of detection	Ref.
H_2O_2			
Au–Ag NPs	15.63–250 μM	—	53
Pt-DNA complexes	0.979–17.6 mM	392 μM	54
Au@TiO_2	5–100 μM	4 μM	15
Au@Ag nanorods	10–10 000 μM	6 μM	55
HRP	1–69 μM	1 μM	56
Core–shell Cu/Au NPs	9.8–625 μM	2.73 μM	This work
Glucose			
Au@Ag nanorods	0.05–20 mM	39 μM	55
Au@TiO_2	0–1 mM	3.5 μM	15
R–Cu@Au/Pt NPs	0–1.9 mM	6 μM	27
Core–shell Cu/Au NPs	0.02–0.67 mM	15 μM	This work

optimized. In the presence of H_2O_2 and TMB, the mixture reacted at room temperature for 5 min. The absorbance was measured at 652 nm with a microplate reader using buffer as blank control. Afterwards, we optimize the reaction time on the reaction system using UV/vis spectrum.

Preparation of BEAS-2B cell lysate samples

BEAS-2B cells (purchased from the cell bank of Shanghai typical culture preservation Committee, Chinese Academy of Sciences) were cultured in DMEM medium containing 10% fetal bovine serum and 100 U/ml penicillin streptomycin, CO_2 concentration of 5%, temperature of 37 °C and humidity of 95% °C. To prepare BEAS-2B cell lysate samples, 3.3×10^5 cells were collected and resuspended with 200 μL KPE buffer (0.1% TritonX-100 and 0.6% sulfosalicylic acid, 0.1 M potassium phosphate buffer, 5 mm EDTA, pH 7.5). Then, the suspension was sonicated for 5 minutes and then centrifuged at 3000 g for 5 minutes. 10 μL of the obtained cell suspension was diluted to 300 μL to prepare for GSH analysis.

H_2O_2 detection using core–shell Cu/Au NPs

Using TMB as substrate, H_2O_2 was quantitatively detected by colorimetric method at room temperature, and the corresponding absorbance values were recorded by Microplate reader (Biotek, USA). Briefly, 100 μL 65 μg mL^{-1} Cu/Au NPs solution and 96 μL 1.5 mM TMB were added into 92 μL 0.2 M HAc-NaAc buffer solution (pH 5) in the 96 well plates. Then, 12 μL H_2O_2 of different concentrations was mixed with the above solution and start timing immediately. After incubating for 20 minutes at room temperature, the absorbance of the solution was measured at 652 nm. LOD is equal to three times the standard deviation of the blank divided by the analytical calibration slope.[50]

Glucose detection using core–shell Cu/Au NPs

10 μL GOx, 10 μL glucose of different concentrations (0.625 to 20 mM), 100 μL 65 μg mL^{-1} core–shell Cu/Au NPs solution and 96

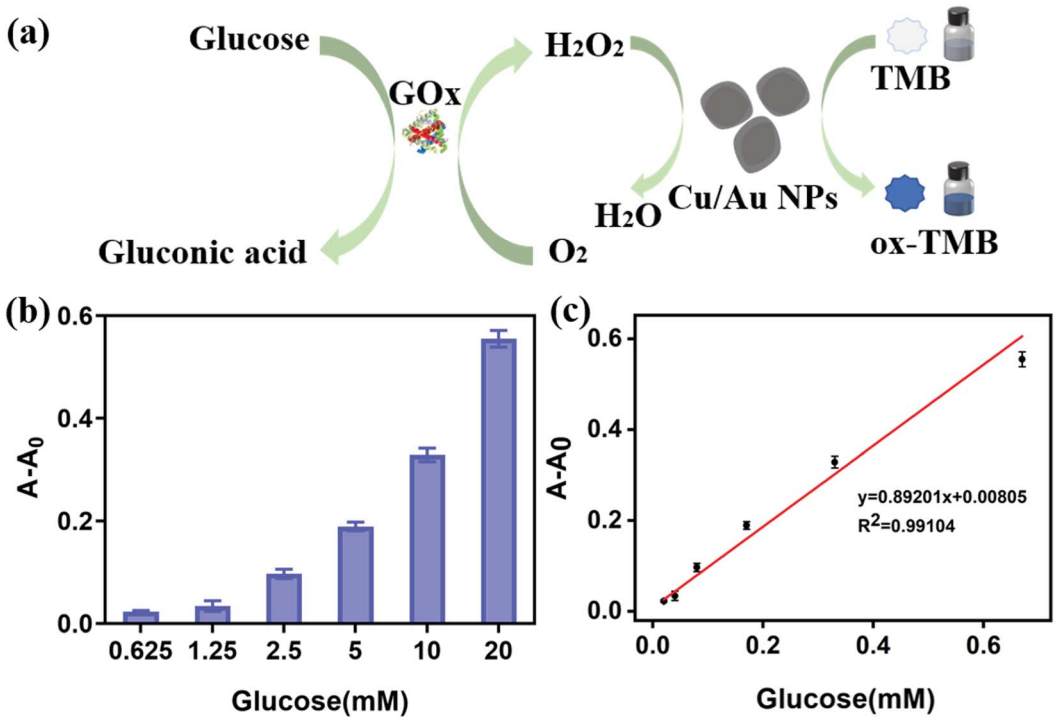

Fig. 6 (a) Schematic illustration of core–shell Cu/Au NPs applied for the colorimetric biosensing of glucose. (b) The dependence of the absorbance on the concentration of glucose in the range from 0.625 to 20 mM. (c) Linear calibration plot for glucose from 20 to 670 μM.

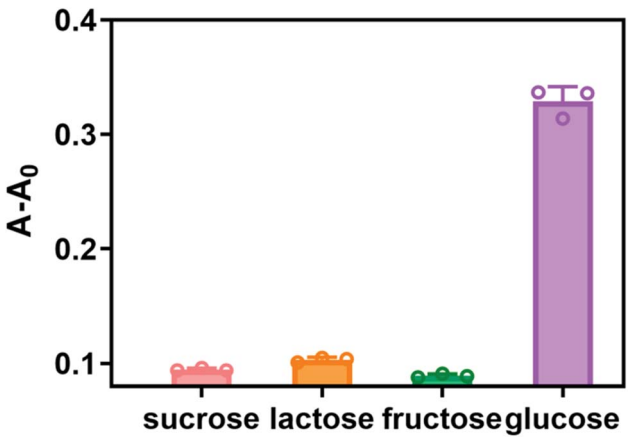

Fig. 7 Selectivity test for glucose detection by the proposed assay. Glucose was 10 mM, the other sugars were 20 mM. Error bars represent the standard deviation of three repeated measurements.

μL 1.5 mM TMB were added into 84 μL 0.2 M HAc-NaAc buffer solution (pH 5) in the 96 well plates. After incubating for 90 minutes at 37 °C, the absorbance values of the solution were measured at 652 nm in a microplate meter (Biotek, USA).

Selectivity of the detection system toward glucose

In order to study the selectivity of the proposed method, sucrose, lactose and fructose were evaluated in the glucose assay. The concentration of glucose was 10 mM, and other three sugars were 20 mM. The detection methods were the same as the detection of glucose.

GSH detection using core–shell Cu/Au NPs

The determination of GSH with colorimetric detection were carried out as followed: 100 μL of 65 μg mL^{-1} core–shell Cu/Au NPs and 12 μL of 0.5 M H_2O_2 were added into 92 μL of HAc-NaAc buffer solution (pH 5). Then 50 μL of varied concentrations of GSH were added. Finally, 96 μL of 1.5 mM TMB were added into the mixture. The change of absorbance at 652 nm was recorded after 10 min of the adding of TMB.

Selectivity of the detection system toward GSH

The influence of a series of biologically relevant amino acids (L-Arg, L-Ala, L-Lys, D-Ala, L-Val, L-Asp), and glucose were evaluated in the GSH assay. The concentrations of L-Arg, L-Ala, L-Lys, D-Ala, L-Val, L-Asp, glucose were 10 mM and GSH was 2 mM, respectively. The detection methods were the same as the detection of GSH.

Detection of glucose and GSH in the spiked samples

For recovery analysis, dissolve commercial biscuits in water to form a solution of 1 mg mL^{-1}, and add 0, 2.5, 5 and 10 mM glucose, respectively. All the spiked samples were performed according to the above colorimetric detection procedure. The recoveries (%) of glucose was analyzed and calculated.

The colorimetric determination of GSH in BEAS-2B cells was carried out according to the above detection method. Briefly speaking, 100 μL of 65 μg mL^{-1} core–shell Cu/Au NPs, 12 μL of 0.5 M H_2O_2 and 92 μL of HAc-NaAc buffer solution (pH 5) were mixed with 50 μL of BEAS-2B Cell Lysate Samples containing

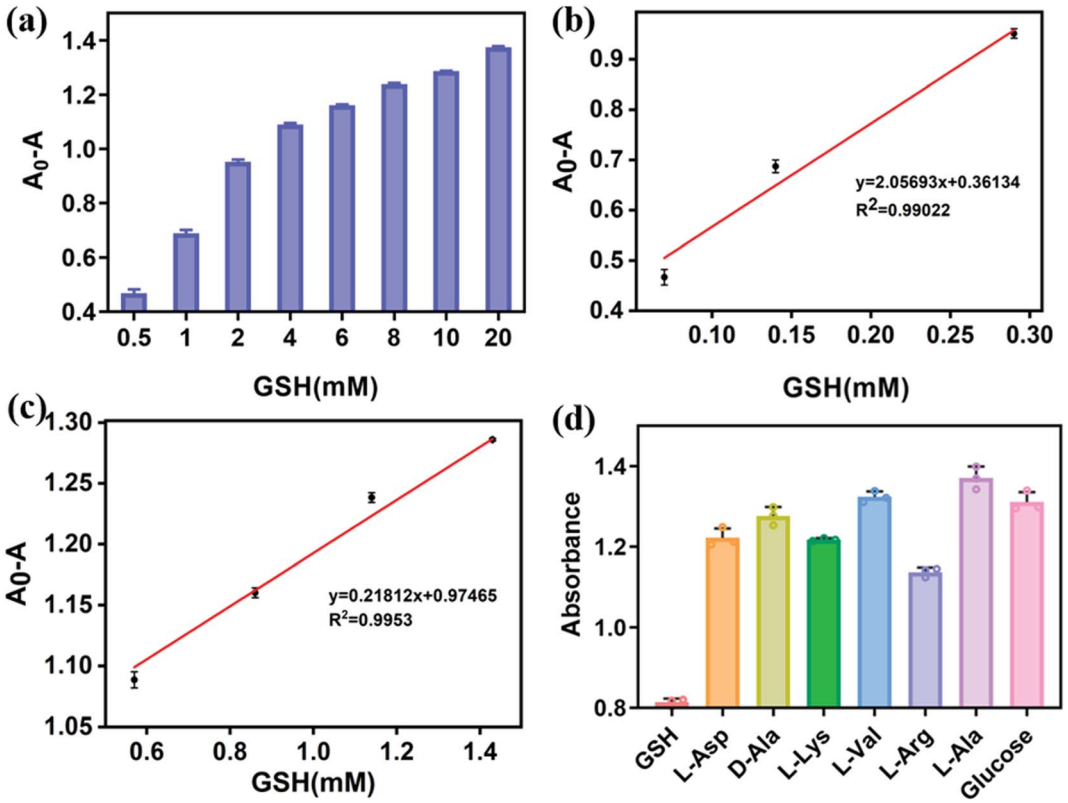

Fig. 8 (a) Linear calibration plot for GSH from 0.5 mM to 10 mM. (b) The dependence of the absorbance on the concentration of GSH in the range from 0.07 to 0.29 mM (b) and 0.57 to 1.43 mM (c). (d) Selectivity test for GSH detection by the proposed assay. GSH was 2 mM, the other amino acids were 10 mM.

Table 2 The recoveries of glucose in the biscuits by the standard addition ($n = 3$)

Sample	Added/mM	Detected/mM	Recovery/%
1	2.5	2.64 ± 0.21	105.56
2	5	5.83 ± 0.19	116.59
3	10	10.82 ± 0.30	108.16

Table 3 The recoveries of GSH in SH-SY5Y Cell Lysate samples ($n = 3$)

Sample	Added/mM	Detected/mM	Recovery/%
1	2	1.91 ± 0.06	95.65
2	4	3.63 ± 0.37	90.76
3	8	7.98 ± 0.34	99.69

varied concentrations of GSH (with final concentrations of 0.29, 0.57, 1.14 mM). Finally, 96 μL of 1.5 mM TMB were added into the mixture. The change of absorbance at 652 nm was recorded after 10 min of the adding of TMB.

Results and discussion

Characterization of iodide-responsive core–shell Cu/Au NPs

According to the literature,[49] core–shell Cu/Au NPs were prepared by reducing $CuSO_4$ and $HAuCl_4$ in the presence of $NaBH_4$ and sodium citrate. The morphology and size of nanoparticles were analyzed by TEM image. As shown in Fig. 1a, core–shell Cu/Au NPs synthesized were non-spherical and interconnected with each other. The structural composition of the particles was determined by estimating the atomic content in the EDX spectrum, and the results showed that Cu and Au coexisted (Fig. 2b). The size distribution result indicated that the diameter was about 7 nm (Fig. 1c). Fig. 1d demonstrated that the hydrodynamic diameter of core–shell Cu/Au NPs was about 26.81 ± 0.15 nm and the surface zeta potential of core–shell Cu/Au NPs was approximately −31.4 ± 1.87 mV. According to previous literature reports,[49] citrate stabilized core–shell Cu/Au NPs can recognize and detect iodine ions with high selectivity. In the presence of iodine ions, interconnected and irregular nanoparticles are transformed into single, separated and approximately spherical nanoparticles, and the solution changed from purple to red. Therefore, iodine recognition colorimetric experiments were carried out at room temperature to verify the successful synthesis of core–shell Cu/Au NPs. Native Cu/Au NPs held a wide absorption band with a maximum absorbance at around 550 nm. And the solution appeared dark purple gray in sunlight. With the increase of iodine ion concentration, the color of the solution gradually changed to light red. The maximum absorption peak changed from 550 nm to 520 nm, and the absorption band became narrower (Fig. 2a). When the Cu/Au NPs were incubated with 10 mM KI for 25 min,

the solution showed light red, and there was a narrowed absorption peak at 520 nm, as displayed in Fig. 2b. This phenomenon was similar with the result of the literature,[6] indicating that core–shell Cu/Au NPs were successfully synthesized.

The peroxidase-mimicking activity of core–shell Cu/Au NPs

Using 3,3′,5,5′-tetramethylbenzidine (TMB) as substrate, the peroxidase-mimicking activity of core–shell Cu/Au NPs was determined by colorimetric method. Fig. 3a demonstrated a colorimetric method for detecting H_2O_2 established on the prepared Cu/Au NPs. In the absence of H_2O_2, Cu/Au NPs did not catalyze TMB to produce blue products ox-TMB, while the color of solution was blue and there was a remarkable peak at 652 nm in the presence of H_2O_2 (Fig. 3b). At the same time, this process was accompanied by color changes visible to the naked eye, as shown in the illustration in Fig. 3c. It can be clearly observed only when core–shell Cu/Au NPs, TMB And H_2O_2 coexist in the reaction, the color of the solution was bright blue, but there was no obvious change in other control systems. The above results indicated that core–shell Cu/Au NPs has peroxidase-mimicking activity.

In order to further explored the peroxidase-mimicking catalytic mechanism of core–shell Cu/Au NPs, the steady-state kinetic analysis was carried out by changing the concentration of H_2O_2 or TMB in the reaction system while keeping the other concentration invariant. We used H_2O_2 and TMB as substrates and kept the core–shell Cu/Au NPs concentration constant throughout the experiment. As demonstrated in Fig. 4a and b, the oxidation reaction catalyzed by the core–shell Cu/Au NPs followed a Michaelis–Menten behavior. Michaelis–Menten constant (K_m) and the maximum reaction rate (V_{max}) can be acquired from Lineweaver–Burk curve and Michaelis–Menten curve. The K_m of core–shell Cu/Au NPs with TMB and H_2O_2 were 1.63 mM and 2.74 mM. The V_{max} of core–shell Cu/Au NPs with TMB and H_2O_2 were 9.80×10^{-8} M S^{-1} and 4.77×10^{-8} M S^{-1}.

Optimization of reaction conditions

Similar to other nano-enzymes, the peroxidase activity of core–shell Cu/Au NPs is decided by reaction pH, temperature and reaction time. Thus, we studied the above factors affecting the catalytic efficiency. As shown in Fig. 5a, the catalytic performance of core–shell Cu/Au NPs gradually enhanced with the increase of pH from 3 to 5, and then decreased with the further increase of pH, indicating that the catalytic activity of Cu/Au NPs was higher in acidic environment. Thereupon, the pH value of 5 was selected in the colorimetric detection. Subsequently, we further optimized the temperature of the reaction system, in order to obtain high catalytic efficiency. With the increase of temperature, the catalytic activity of core–shell Cu/Au NPs and the absorbance of the reaction system decreased (Fig. 5b). When the reaction temperature was in the range of 25–45 °C, the catalytic efficiency of Cu/Au NPs was similar. For the convenience of the experiment, we chose 25 °C for the follow-up experiment. As shown in Fig. 5c, we optimized the reaction time to detect hydrogen peroxide. The result exhibited that the absorbance increased gradually with the extension of time. When the reaction time was 20 min, the absorbance tended to be stable. Hence, we chose 20 min as the reaction time to detect hydrogen peroxide.

Calibration curve for H_2O_2 detection

Under the determined optimal experimental conditions, the catalysis-based colorimetric assay displayed absorption changes with different concentrations of H_2O_2.

As shown in Fig. 5d, with the increase of H_2O_2 concentration, the absorbance of the solution increased gradually. The correlation between the absorbance values and H_2O_2 concentration were linear over the range of 9.8–625 μM with a correlation coefficient of 0.9984. The lower limit of detection (LOD) of core–shell Cu/Au NPs for H_2O_2 was found to be 2.73 μM (3σ/S). The analytical performance of Cu/Au NPs as peroxidase mimetic enzyme was compared with other nano-enzymes, as shown in Table 1. Compared with other nano-enzymes, the constructed sensor has considerable detection range and sensitivity. Moreover, this method of synthesizing nanoparticles is simple and mild, and is expected to become a candidate method for H_2O_2 detection.

Calibration curve for glucose detection

It is well known that colorimetric detection method is widely used to prepare highly sensitive and selective sensors because of its simplicity, low cost and no need for complex instruments, and the color change in the reaction process can be observed by naked eyes.[51] Considering the above advantages, we established a simple glucose detection method (Fig. 6a). In the presence of glucose, GO*x* can catalyze glucose to produce gluconic acid and H_2O_2. Subsequently, H_2O_2 and core–shell Cu/Au NPs oxidize TMB to blue ox-TMB, so as to realize the visual detection of glucose. With the increase of glucose content, the absorbance at around 652 nm enhanced gradually (Fig. 6b). The correlation between the absorbance values and glucose concentration was linear over the range of 20–670 μM with a correlation coefficient of 0.9910 (Fig. 6c). The lower limit of detection (LOD) of core–shell Cu/Au NPs for glucose was found to be 15 μM (3σ/S). Compared with the previously reported colorimetric method for glucose detection, our proposed method has considerable linear range and sensitivity (Table 1). And compared with other methods, Au@TiO_2 [15]and R–Cu@Au/Pt NPs[50] have lower detection limits, but the synthesis method of Au@TiO_2 is complex and Pt is a relatively expensive metal material, which would increase the cost accordingly. This method has some advantages in glucose detection because of its simple operation and low cost.

Selectivity of the detection system toward glucose

To evaluate the selectivity detection system for glucose, the investigations were carried out with three sugars including sucrose, lactose and fructose. And the concentrations of the other three sugars were two times higher than that of glucose. As shown in Fig. 7, compared with the other three sugars, the absorbance value increased significantly in the presence of

glucose, but the other three substances were difficult to detect changes in absorbance. The above results indicated that our method has high selectivity for glucose detection.

Calibration curve for GSH detection

Under the optimized conditions, different concentrations of GSH were introduced into the core–shell Cu/Au NPs peroxidase reaction system to evaluate the analytical performance of the sensor, including linear response range and detection limit, as shown in Fig. 8. With the increase of GSH concentration, the value of $A_0 - A$ (A_0 and A refer to the absorbance value in the absence and presence of GSH) gradually increased (Fig. 8a). The correlation between the absorbance values and GSH concentration was linear over the range of 0.07 to 1.43 mM with a correlation coefficient of 0.9902 and 0.9953 (Fig. 8b and c). The lower limit of detection (LOD) of Cu/Au NPs for GSH was found to be 13 μM (3σ/S). Colorimetric detection of GSH has been widely concerned because of its simple operation, low cost and high sensitivity. In addition, nano-enzyme is a promising material for the detection of GSH.[52] Compared with other materials for the detection of GSH, the performance of our colorimetric method is equivalent to that of other methods. Moreover, the synthesis method of Cu/Au NPs is simple, which is expected to be an ideal material for the detection of GSH.

Selectivity of the detection system toward GSH

Selectivity is also an important factor in evaluating the performance of the proposed method. To better simulate the intracellular, some potential interfering substances including L-Arg, L-Ala, L-Lys, D-Ala, L-Val, L-Asp and glucose were investigated in the detection. As shown in Fig. 8d, the proposed method displays high selectivity for the detection of GSH.

Detection of glucose and GSH in the spiked samples

To evaluate the accuracy and practicality of the established method, glucose with different concentrations were further detected in the spiked samples by conducting three replicate analyses. As shown in Table 2, the average recoveries were in the range of 105–116%. Therefore, this colorimetric method is applicable to real samples to determine glucose concentration.

In order to verify the detection performance of the proposed detection in real samples, GSH in BEAS-2B cell samples was detected. The BEAS-2B cell lysate samples were diluted to be consistent with the linear response range of our proposed colorimetric method. The recovery experiment was carried out by standard addition method, the average recovery was from 90% to 100%, as shown in Table 3. This result indicated that our method has great potential in detecting GSH in real samples.

Conclusions

In summary, we successfully synthesized and characterized core–shell Cu/Au NPs, and developed a colorimetric assay for H_2O_2, glucose and GSH detection. Under the optimal experimental conditions, the method displayed good responses toward H_2O_2 with a linear range from 9.8 to 625 μM. The LOD value was 2.73 μM. Determination of glucose was achieved from 20–670 μM with a LOD of 15 μM. For the detection of GSH, the linear range was from 0.07 to 1.43 mM with a LOD of 13 μM. The above results showed that the proposed method had a wide linear range for the detection of H_2O_2, glucose and GSH, and was fast, simple and sensitive. And this method can be used for the detection of actual samples, and has great application potential in environmental monitoring and clinical diagnosis.

Conflicts of interest

The authors declare that they have no known competing financial interests or personal relationships that could have appeared to influence the work reported in this paper.

Acknowledgements

This work was financially supported by NSFC (82073602). National Natural Science Foundation of Jilin Province (20200201081JC).

References

1 G. Cabello, K. C. Nwoko, J. F. Marco, M. Sánchez-Arenillas, A. M. Méndez-Torres, J. Feldmann, C. Yáñez and T. A. D. Smith, *J. Alloys Compd.*, 2019, **791**, 184–192.
2 V. Raj, T. Johnson and K. Joseph, *Biosens. Bioelectron.*, 2014, **60**, 191–194.
3 R. S. Dey and C. R. Raj, *ACS Appl. Mater. Interfaces*, 2013, **5**, 4791–4798.
4 J. S. Lee, M. S. Han and C. A. Mirkin, *Angew. Chem., Int. Ed. Engl.*, 2007, **46**, 4093–4096.
5 X. Zhang, P. Geng, H. Liu, Y. Teng, Y. Liu, Q. Wang, W. Zhang, L. Jin and L. Jiang, *Biosens. Bioelectron.*, 2009, **24**, 2155–2159.
6 T. Lou, H. Qiang and Z. Chen, *Talanta*, 2017, **163**, 132–139.
7 X. Ye, H. Shi, X. He, K. Wang, D. He, L. Yan, F. Xu, Y. Lei, J. Tang and Y. Yu, *Anal. Chem.*, 2015, **87**, 7141–7147.
8 C. Jiang, J. Zhu, Z. Li, J. Luo, J. Wang and Y. Sun, *RSC Adv.*, 2017, **7**, 44463–44469.
9 D. Zhao, C. Chen, L. Lu, F. Yang and X. Yang, *Sens. Actuators, B*, 2015, **215**, 437–444.
10 Y. Chang, Z. Zhang, J. Hao, W. Yang and J. Tang, *Sens. Actuators, B*, 2016, **232**, 692–697.
11 Y. Liu, D. Ding, Y. Zhen and R. Guo, *Biosens. Bioelectron.*, 2017, **92**, 140–146.
12 S. Bhagat, N. V. Srikanth Vallabani, V. Shutthanandan, M. Bowden, A. S. Karakoti and S. Singh, *J. Colloid Interface Sci.*, 2018, **513**, 831–842.
13 F. Shah, N. Yadav and S. Singh, *Colloids Surf., B*, 2021, **198**, 111478.
14 V. Jain, S. Bhagat, M. Singh, V. Bansal and S. Singh, *RSC Adv.*, 2019, **9**, 33195–33206.
15 X. Peng, G. Wan, L. Wu, M. Zeng, S. Lin and G. Wang, *Sens. Actuators, B*, 2018, **257**, 166–177.
16 L. Shen, C. Chu, C. Ma, H. Yang, S. Ge, J. Yu, M. Yan and X. Song, *Sens. Actuators, B*, 2014, **201**, 196–203.

17 T. Sasikumar and M. Ilanchelian, *Opt. Mater.*, 2020, **109**, 110237.
18 P. Lignier, R. Bellabarba and R. P. Tooze, *Chem. Soc. Rev.*, 2012, **41**, 1708–1720.
19 C. Liu, Y. Cai, J. Wang, X. Liu, H. Ren, L. Yan, Y. Zhang, S. Yang, J. Guo and A. Liu, *ACS Appl. Mater. Interfaces*, 2020, **12**, 42521–42530.
20 Y. Zhang, S. Yang, J. Wang, Y. Cai, L. Niu, X. Liu, C. Liu, H. Qi and A. Liu, *Talanta*, 2021, **233**, 122594.
21 F. Nie, L. Ga, J. Ai and Y. Wang, *RSC Adv.*, 2018, **8**, 13708–13713.
22 Y. Tao, E. Ju, J. Ren and X. Qu, *Chem. Commun.*, 2014, **50**, 3030–3032.
23 J. Sun, C. Li, Y. Qi, S. Guo and X. Liang, *Sens.*, 2016, **16**, 584.
24 R. Tian, B. Zhang, M. Zhao, H. Zou, C. Zhang, Y. Qi and Q. Ma, *RSC Adv.*, 2019, **9**, 12209–12217.
25 M. Hussain, A. Nisar, L. Qian, S. Karim, M. Khan, Y. Liu, H. Sun and M. Ahmad, *Nanotechnology*, 2021, **32**, 205501.
26 Q. Chang and H. Tang, *Microchim. Acta*, 2014, **181**, 527–534.
27 C. Jiang, X. Wei, S. Bao, H. Tu and W. Wang, *RSC Adv.*, 2019, **9**, 41561–41568.
28 A. K. Rines, K. Sharabi, C. D. Tavares and P. Puigserver, *Nat. Rev. Drug Discovery*, 2016, **15**, 786–804.
29 R. Tian, J. Sun, Y. Qi, B. Zhang, S. Guo and M. Zhao, *Nanomaterials*, 2017, **7**(11), 347.
30 W. Na, H. Liu, M. Wang and X. Su, *Microchim. Acta*, 2017, **184**, 1463–1470.
31 S. K. Vaishanav, J. Korram, R. Nagwanshi, K. K. Ghosh and M. L. Satnami, *Sens. Actuators, B*, 2017, **245**, 196–204.
32 Q. Chen, Y. Fu, W. Zhang, S. Ye, H. Zhang, F. Xie, L. Gong, Z. Wei, H. Jin and J. Chen, *Talanta*, 2017, **165**, 516–521.
33 C. H. Wang, C. Yang, Y. Y. Song, W. Gao and X. H. Xia, *Adv. Funct. Mater.*, 2005, **15**, 1267–1275.
34 D. Lan, B. Li and Z. Zhang, *Biosens. Bioelectron.*, 2008, **24**, 940–944.
35 Q. Chang, L. Zhu, G. Jiang and H. Tang, *Anal. Bioanal. Chem.*, 2009, **395**, 2377–2385.
36 D. Fink, I. Klinkovich, O. Bukelman, R. S. Marks, A. Kiv, D. Fuks, W. R. Fahrner and L. Alfonta, *Biosens. Bioelectron.*, 2009, **24**, 2702–2706.
37 H. Wei and E. Wang, *Chem. Soc. Rev.*, 2013, **42**, 6060–6093.
38 R. Lv, X. Zhang, R. Sun, L. Chen, Y. Zhang, R. Sheng, T. Du, Y. Li and Y. Qi, *Particuology*, 2022, **64**, 178–185.
39 J. Yue, Q. Mei, P. Wang, P. Miao, W. F. Dong and L. Li, *ACS Appl. Mater. Interfaces*, 2022, **14**, 17119–17127.
40 X. Zhang, F. G. Wu, P. Liu, N. Gu and Z. Chen, *Small*, 2014, **10**, 5170–5177.
41 F. Gong, L. Cheng, N. Yang, Q. Jin, L. Tian, M. Wang, Y. Li and Z. Liu, *Nano Lett.*, 2018, **18**, 6037–6044.
42 A. Song, T. Feng, X. Shen, S. Gai, Y. Zhai and H. Chen, *Chem. Commun.*, 2019, **55**, 7219–7222.
43 Y. Shi, Y. Pan, H. Zhang, Z. Zhang, M. J. Li, C. Yi and M. Yang, *Biosens. Bioelectron.*, 2014, **56**, 39–45.
44 Y. Huang, Y. Zhang, F. g. Huo, Y. Liu and C. Yin, *Sens. Actuators, B*, 2019, 301.
45 J. Ou-Yang, C. Y. Li, Y. F. Li, J. Fei, F. Xu, S.-J. Li and S.-X. Nie, *Sens. Actuators, B*, 2017, **240**, 1165–1173.
46 Z. Z. Dong, L. Lu, C. N. Ko, C. Yang, S. Li, M. Y. Lee, C. H. Leung and D. L. Ma, *Nanoscale*, 2017, **9**, 4677–4682.
47 C. Wang, L. Chen, P. Wang, M. Li and D. Liu, *Biosens. Bioelectron.*, 2019, **133**, 154–159.
48 L. Han, S. G. Liu, J. Y. Liang, N. B. Li and H. Q. Luo, *Sens. Actuators, B*, 2019, **288**, 195–201.
49 J. Zhang, X. Xu, C. Yang, F. Yang and X. Yang, *Anal. Chem.*, 2011, **83**, 3911–3917.
50 P. Wu, P. Ding, X. Ye, L. Li, X. He and K. Wang, *RSC Adv.*, 2019, **9**, 14982–14989.
51 P. Li, J. Zheng, J. Xu and M. Zhang, *Dalton Trans.*, 2021, **50**, 14753–14761.
52 B. Zhang, H. Zou, Y. Qi, X. Zhang, R. Sheng, Y. Zhang, R. Sun, L. Chen and R. Lv, *Microchem. J.*, 2021, **164**, 106013.
53 X. Jiang, X. Fan, W. Xu, R. Zhang and G. Wu, *ACS Biomater. Sci. Eng.*, 2020, **6**, 680–689.
54 X. Chen, X. Zhou and J. Hu, *Anal. Methods*, 2012, **4**, 2183–2187.
55 L. Han, C. Li, T. Zhang, Q. Lang and A. Liu, *ACS Appl. Mater. Interfaces*, 2015, **7**, 14463–14470.
56 E. P. a. Y. Keisari, *J. Immunol. Methods*, 1980, **38**, 161–170.